Voxel-Based Analysis of ^{11}C-PIB Scans for Diagnosing Alzheimer's Disease

Arthur Mikhno[1], Davangere Devanand[2,3], Gregory Pelton[2,3], Katrina Cuasay[3], Roger Gunn[4], Neil Upton[4], Robert Y. Lai[4], Vincenzo Libri[4], J. John Mann[1,2], and Ramin V. Parsey[1,2]

[1]Department of Molecular Imaging and Neuropathology, New York State Psychiatric Institute, New York, New York; [2]Columbia University, New York, New York; [3]Department of Geriatric Depression, New York State Psychiatric Institute, New York, New York; and [4]GlaxoSmithKline CPDM and Neurology-CEDD, Essex, United Kingdom

The positron emission tomography (PET) radioligand *N*-methyl-^{11}C-2-(4-methylaminophenyl)-6-hydroxybenzothiazole (also known as ^{11}C-6-OH-BTA-1 or ^{11}C-PIB) binds to amyloid-β (Aβ), which accumulates pathologically in Alzheimer's disease (AD). Although ^{11}C-PIB accumulation is greater in patients with AD than in healthy controls at a group level, the optimal method for discriminating between these 2 groups has, to our knowledge, not been established. We assessed the use of data-determined standardized voxels of interest (VOIs) to improve the classification capability of ^{11}C-PIB scans on patients with AD. **Methods:** A total of 16 controls and 14 AD age-matched patients were recruited. All subjects underwent a ^{11}C-PIB scan and structural MRI. Binding potential (a measure of amyloid burden) was calculated for each voxel using the Logan graphical method with cerebellar gray matter as the reference region. Voxel maps were then partial-volume corrected and spatially normalized by MRI onto a standardized template. The subjects were divided into 2 cohorts. The first cohort (control, 12; AD, 9) was used for statistical parametric mapping analysis and delineation of data-based VOIs. These VOIs were tested in the second cohort (control, 4; AD, 5) of subjects. **Results:** Statistical parametric mapping analysis revealed significant differences between control and AD groups. The VOI map determined from the first cohort resulted in complete separation between the control and the AD subjects in the second cohort ($P < 0.02$). Binding potential values based on this VOI were in the same range as other reported individual and mean cortical VOI results. **Conclusion:** A standardized VOI template that is optimized for control or AD group discrimination provides excellent separation of control and AD subjects on the basis of ^{11}C-PIB uptake. This VOI template can serve as a potential replacement for manual VOI delineation and can eventually be fully automated, facilitating potential use in a clinical setting. To facilitate independent analysis and validation with more and a broader variety of subjects, this VOI template and the software for processing will be made available through the Internet.

Key Words: PET; PIB; Alzheimer's; diagnosis; voxel

J Nucl Med 2008; 49:1262–1269
DOI: 10.2967/jnumed.107.049932

Received Dec. 17, 2007; revision accepted Apr. 16, 2008.
For correspondence or reprints contact: Arthur Mikhno, 1051 Riverside Dr., Manhattan, NY 10032.
E-mail: am2679@columbia.edu

Alzheimer's disease (AD) is characterized by memory loss, cognitive impairment, and behavioral changes. It is estimated that more than 15 million people worldwide have this disease, and it is the seventh leading cause of death in the United States (*1*). In the United States, diagnosis is made on the basis of clinical examination using the National Institute of Neurological and Communicative Disorders and Stroke/Alzheimer's Disease and Related Disorders Association criteria. This method ranges from 76% to 98% sensitivity and from 61% to 84% specificity (*2*). The wide range partly depends on the stage of the disease at the time of examination and clinician skill. Clinical diagnosis is more accurate in later stages of the disease, whereas diagnosis is more difficult in early-stage AD.

AD pathology is characterized by extracellular amyloid β (Aβ) neuritic plaques and intracellular neurofibrillary tangles. Aβ plaques are thought to be toxic and result in neuronal loss and cortical atrophy. It has been shown that Aβ progressively accumulates in the brain throughout the duration of the disease. Excessive Aβ accumulation eventually involves much of the neocortex, hippocampus, and many subcortical structures. Clinical symptoms appear after significant deposition of Aβ has already occurred (*3*). With the advent of potential new therapeutic agents that work by arresting Aβ accumulation or by depleting Aβ levels in the brain, sensitive and specific detection of early-stage AD, before significant impairment has occurred, is crucial to early treatment and prevention of disease progression.

With the development of the radioligand *N*-methyl-^{11}C-2-(4-methylaminophenyl)-6-hydroxybenzothiazole (also known as ^{11}C-PIB or ^{11}C-6-OH-BTA-1) for positron emission tomography (PET), it is now possible to visualize the uptake pattern and to quantify the amount of Aβ present in the brain (*4*). Several groups have shown that healthy controls and patients with AD exhibit differential ^{11}C-PIB uptake (*4–7*). However, some of these reports show an overlap between the groups in the frontal or prefrontal cortex (*4,7*), whereas several show an overlap in other regions (*4,6,7*). Potential postulates for this overlap include

incorrect clinical diagnosis of AD (*2*), controls who have incipient AD, unknown ligand specificity (*8*), partial-volume effects (*9,10*), inappropriate quantification model (*8,11*), and the variability and specificity of the anatomic voxels of interests (VOIs) that have been used to delineate and quantify Aβ binding. Aβ formation does not adhere to the boundaries of traditional anatomic regions (*3*). For this reason, VOIs that have commonly been analyzed (prefrontal, temporal, precuneus, and striatum) might not be optimal regions for diagnosis. Alternative approaches have included total cortical Aβ binding (*5,12*) or visual assessment by a radiologist (*12*). The cortical binding measure elicits differences between the groups. The studies that reported this measure differed in their outcomes. In one study (*5*), total group separation was observed, though the highest control and lowest AD subjects were separated by a distance of only 0.02 binding potential (BP_{ND}) units. In the other studies (*6,12*), several controls and patients with AD overlapped in their mean cortical binding. Visual diagnosis made on the basis of a ^{11}C-PIB scan performed by 2 trained raters showed 100% sensitivity and varied (80%–88%) in specificity (*12*). Although this strategy might be effective in ensuring that true patients with AD are diagnosed, it is still prone to a significant false-positive rate; relies on trained radiologist availability, level, or training; and is susceptible to interrated and intrarater variability. This difference in outcome is evident in the above study, in which the less-experienced radiologist scored 8% lower in specificity than the more experienced one.

In this study, we sought to determine whether the sensitivity and specificity of healthy control and AD discrimination can be improved through empiric or data-based derivation of standardized VOIs from ^{11}C-PIB scans. To increase the signal or noise of our VOIs, we derived them from partial-volume–corrected data. Standardized VOIs have the additional advantage of being consistent and not susceptible to rater availability, training, and variability. The objective of this strategy is to establish a simple, quick, semiautomatic way of discriminating between controls and patients with AD. The current study is an initiative to develop automatic screening methods using ^{11}C-PIB data for clinical and research purposes.

To create the standardized VOI set, we derived voxelwise ^{11}C-PIB BP_{ND} partial-volume–corrected cortical gray matter images that were generated from a set of controls (n = 12) and patients with AD (n = 9). We used statistical parametric mapping (SPM), extracting the voxels at different statistical significance thresholds and, each time, reapplying them to the initial data to derive mean cortical binding values. The resulting binding, at different thresholds, was evaluated for group separation and whether some of the overlap found between control and AD groups would be qualified by the use of these new regions, to better support the clinical diagnosis. Finally, the most effective VOI set was tested prospectively in a new cohort of controls (n = 4) and patients with AD (n = 5).

MATERIALS AND METHODS

Subjects

A total of 16 controls and 14 patients with AD were recruited for this study. All participants signed informed consent in this institutional review board–approved protocol. Patients presented with memory complaints to a Memory Disorders Clinic jointly run by the Departments of Psychiatry and Neurology at New York State Psychiatric Institute and Columbia University. AD samples were obtained from this pool of patients. Patients with AD met National Institute of Neurological and Communicative Disorders and Stroke/Alzheimer's Disease and Related Disorders Association criteria for probable AD (*13*). Healthy controls were recruited primarily by advertisement, were required to have normative Mini-Mental State Examination and selective reminding test scores, had to meet all other patient inclusion or exclusion criteria, and were group-matched to patients on the basis of age and sex. Subjects were divided into 2 control and AD cohorts, cohort 1 and cohort 2. Cohort 1 (control, 12; AD, 9) was used for SPM analysis and VOI development, and cohort 2 (control, 4; AD, 5) was used for testing and evaluation of the VOIs derived from cohort 1. Cohort 1 consisted of all subjects available for development at its onset, and cohort 2 consisted of new subjects whose data were acquired consecutively after methods development. Demographic information for cohorts 1 and 2 is shown in Table 1.

^{11}C-PIB Synthesis

The full radiosynthesis of ^{11}C-PIB is described elsewhere (*14*). Briefly, ^{11}C-methyl trifluoromethansulfonate was trapped into an acetone (400 μL) solution containing 0.5 mg of 2-(4-aminophenyl)-6-hydroxybenzothiazole at room temperature. The resulting mixture was allowed to react at 60°C for 2 min and allowed to cool to room temperature. The crude product was

TABLE 1
Demographic Data for Cohorts 1 and 2

Data	Cohort 1 (initial SPM analysis)		Cohort 2 (method evaluation only)	
	control (n = 12)	AD (n = 9)	control (n = 4)	AD (n = 5)
Age	71.5 ± 8.4	65.9 ± 8.5	67.8 ± 9.2	65.9 ± 8.5
Male/female	6/6	3/6	2/2	2/3
MMSE	28.8 ± 0.9	21.4 ± 3.6	28.3 ± 1.0	22 ± 1.6
Dose (MBq)	426 ± 151	491 ± 181	644 ± 75	448 ± 173

Data are means ± SDs. MMSE = Mini-Mental State Examination Score.

loaded into a semipreparative high-performance liquid chromatography column (C18; Phenomenex) and eluted with 40:60 (acetonitrile:water, 0.1 M ammonium formate and 0.5% acetic acid, 10 mL/min); the product fraction was collected between 7 and 8 min based on a radiation detector. The collected fraction was then diluted with deionized water (100 mL), passed through a C18 SepPak (Waters), and washed with water (10 mL); the product was then eluted from the SepPak with 1 mL of ethanol. A small portion of the product was analyzed with analytic high-performance liquid chromatography for chemical and radiochemical purities and specific activity. The remaining ethanol solution was diluted with 9 mL of normal saline, filtered through a 0.22-μm filter, and used for further studies. The average yield was found to be 14.5% at the end of synthesis, with a specific activity greater than 37 GBq/mmol.

PET

A polyurethane head immobilizer molded around the subject's head minimized movement. PET images were acquired on an ECAT EXACT HR+ scanner (Siemens/CTI). Before injection, a 10-min transmission scan was performed. At the end of the transmission scan, between 185 and 740 MBq of ^{11}C-PIB were administered intravenously as a bolus for 30 s. Emission data were collected in 3-dimensional mode for 90 min, binning over 18 frames of increasing duration (3 × 20 s, 3 × 1 min, 3 × 2 min, 2 × 5 min, and 7 × 10 min). Images were reconstructed to a 128 × 128 matrix (pixel size, 2.5 × 2.5 mm). Reconstruction was performed with attenuation correction using the transmission data, and scatter correction was performed using a model-based approach (*15*). The reconstruction and estimated image filters were Shepp 0.5 (2.5-mm full width at half maximum [FWHM]; Siemens/CTI), the Z filter was all-pass 0.4 (2.0 FWHM; Siemens/CTI), and the zoom factor was 4.0, leading to a final image resolution of 5.1-mm FWHM at the center of the field of view (*16*).

MRI

MR images were acquired using a 1.5- or a 3-T system (Signa Advantage; GE Healthcare). All scans from the 1.5-T camera were acquired in the coronal plane (orthogonal to the anterior commissure–posterior commissure plane over the whole brain) with the following parameters: 3-dimensional spoiled gradient-recalled acquisition in the steady state; repetition time, 34 ms; echo time, 5 ms; flip angle, 45°; 1.5-mm slice thickness (zero gap); 124 slices; and field of view, 220 × 160 mm. All images from the 1.5-T camera were reconstructed to a size of 256 × 256, with a resolution of 1.5 × 0.86 × 0.86 mm. Scans from the 3-T camera were acquired with the following parameters: repetition time, 5.4 ms; echo time, 2.1 ms; flip angle, 11°; 1-mm slice thickness (zero gap); 160 slices; and field of view, 256 × 256 mm. All images from the 3-T camera were reconstructed to a size of 256 × 256, with an isotropic resolution of 1 × 1 × 1 mm.

Image Analysis Platform

Image analysis was performed using Matlab 2006b (The Mathworks), with extensions to the following open-source packages: Functional MRI of the Brain's Linear Image Registration Tool (FLIRT), version 5.2 (*17*); Brain Extraction Tool (BET), version 1.2 (*18*); and University College of London's Statistical Parametric Mapping (SPM5) normalization (*19*) and segmentation routines (*20*).

PET Image Processing

To correct for subject motion during the PET scan, denoising filter techniques were applied to all PET images starting at frame 5. Frame 8 was used as a reference to which all other frames were aligned using rigid-body FLIRT. The effectiveness of motion correction was assessed by viewing a combined movie of before and after motion correction in the sagittal, axial, and coronal views. Motion was evaluated for drift between frames and across the entire scan duration separately. For registration, a mean of the motion-corrected frames 8 through 18 was registered, using FLIRT, to each subject's BET skull stripped MRI. The resultant transform was applied to the entire motion-corrected PET dataset to bring the images into MRI space. A mean of the MRI-space PET images was then created. This mean image was overlaid onto the MR image to evaluate coregistration.

Derivation of Cerebellar Time–Activity Data

A region of interest (ROI) was drawn on the MR image, which included the entire cerebellum (volume, 121 ± 14 cm^3). A binary mask of this ROI was then created. To correct the cerebellar ROI to include gray matter, only unprocessed MR images were segmented using SPM5 to derive the probabilistic gray matter (GM_p) map. The GM_p map and all individual PET frames were multiplied (masked) by the cerebellar binary mask. On a frame-by-frame basis, the sum of all voxels in each masked PET image was divided by the sum of all voxels in the masked GM_p map to derive the gray matter cerebellar time–activity curve.

PET Modeling

BP_{ND} maps were generated using the Logan graphical method (*21*) from 90-min PET data. The gray matter probability-corrected time–activity curve of the cerebellum was used as a reference. The cerebellum has been shown to be nearly devoid of amyloid plaques in postmortem analysis (*22*) and also shows little ^{11}C-PIB retention in controls and AD (*4*). The Logan method is stable, has high test–retest reliability (*23*), and is sensitive to small changes in ^{11}C-PIB when compared with quantification using an arterial input function (*11*). Furthermore, several investigators (*7,12,23,24*) have suggested the use of the Logan method in deriving BP_{ND} voxel maps, despite its well-documented noise-dependent bias (*8,25,26*).

Partial-Volume Correction (PVC)

Regions that share a border with lower- or higher-binding structures are susceptible to partial-volume effects due to a blurring caused by the low resolution of PET (*27*). Because gray matter, white matter, and cerebrospinal fluid (CSF) have different ^{11}C-PIB uptake patterns (*4*), all gray matter borders undergo partial-volume effects. Atrophy of a region that increases the amount of neighboring CSF increases the partial-volume effects, and cortical atrophy in AD is well established (*28*). Applying PVC to AD data has been shown to increase the signal from atrophied tissue in ^{18}F-FDG (*29*) and SPECT (*9*) scans. In one ^{18}F-FDG study (*29*), signal increase after PVC ranged from 16% to 38% in controls and 19% to 49% in AD. Therefore, we performed all analyses on PVC ^{11}C-PIB binding data.

Voxel BP_{ND} maps were transformed onto the MRI space using the PET-to-MRI coregistration parameters described above. The maps were then corrected for partial volume using a 3-compartment method (*30*). A spherically symmetric point spread function with a FWHM of 5.1 mm was assumed (*16*), and the white matter mean value was obtained by using the geometric transfer matrix method

with 3 compartments (GM_p, WM_p, and CSF_p), as previously suggested (*10*). We used 3-compartment PVC because it recovers more gray matter tracer concentration than the 2-compartment (gray matter and CSF) approach (*30,31*). Although it has been suggested that the 3-compartment approach is more susceptible to coregistration and motion-correction errors (*31*), we were able to take advantage of improved methodologic and evaluation techniques to minimize this effect.

PET Normalization

Each individual's unprocessed MR image was normalized using SPM5 to the International Consortium for Brain Mapping 152-subject, 8-mm smoothed T1 template (*32,33*). MRI space PVC BP_{ND} maps (MRI-BP_{ND}-PVC) were shadow-transformed onto each individual's Montreal Neurological Institute (MNI) normalized MRI (MNI-BP_{ND}-PVC) using the resulting transform parameters.

SPM Analysis

Analysis was executed using the first cohort of subjects (control, 12; AD, 9) in SPM5, using their MNI-BP_{ND}-PVC images. Before analysis, all images were smoothed using an 8-mm FWHM gaussian kernel. A Student *t* test was then done, assuming independence and unequal variance with no covariates or masking. Grand-mean scaling or global normalization was not applied, as BP_{ND} is an absolute measurement. The *t* map, *t* score threshold for *P* values ranging from 0.5 to 1.0E−12, was obtained at an extent threshold of 0 voxels.

SPM-Derived VOI Analysis

The *t* score thresholds from the SPM analysis were applied to the SPM *t* map voxel image by setting all voxels less than a particular threshold to 0. Setting all remaining voxels greater than 0 to 1 created binary masks of the *t* map image. For each threshold, the corresponding binary mask was inverse-transformed into each subject's native MRI space and treated as a VOI mask. Multiplying the VOI mask by each subject's GM_p and MRI-BP_{ND}-PVC map created a cortical binding map. The sum of the entire resulting image was divided by the mean of the GM_p to derive a mean cortical BP_{ND} value for the VOI. This was repeated for each subject in the first cohort. For each VOI, we performed a Student *t* test between BP_{ND} results of first-cohort control ($n = 12$) and AD ($n = 9$) groups that were used to create the *t* score map. By doing this, we empirically determined which *t* score threshold and hence VOI gave the best separation.

Evaluation

To test the effectiveness of the best *t* map threshold–derived VOI mask, created from the analysis described above, we applied the mask to MRI-BP_{ND}-PVC images of a second cohort of control ($n = 4$) and AD ($n = 5$) subjects.

RESULTS

Comparison of ^{11}C-PIB BP_{ND} Between Controls and Patients with AD

The resulting *t* score map ($t = 3.61$, $P < 1E-4$, uncorrected) from the SPM comparison of the first cohort (control, 12; AD, 9) is shown in Figure 1 (top). The areas with significant differences are localized to the frontal, parietal, insular, temporal, and precuneus cortices.

Creation and Evaluation of Data-Derived VOIs

SPM maps were made into binary masks, using different *t* score thresholds, and reapplied as VOIs to the control ($n = 12$) and AD ($n = 9$) MRI-BP_{ND}-PVC maps of the first cohort. Three representative *t* maps, thresholded at different *t* scores, are shown as cortical projections on a rendering of a single subject's T1-weighted MR image (Fig. 1). Red areas for a given threshold represent the extent of the VOI used to calculate mean cortical binding.

Mean cortical BP_{ND} from controls and patients with AD derived from each VOI are shown as scatter plots underneath their corresponding *t* map (Fig. 1, bottom). *P* values determined by Student *t* test between the groups at different *t* score

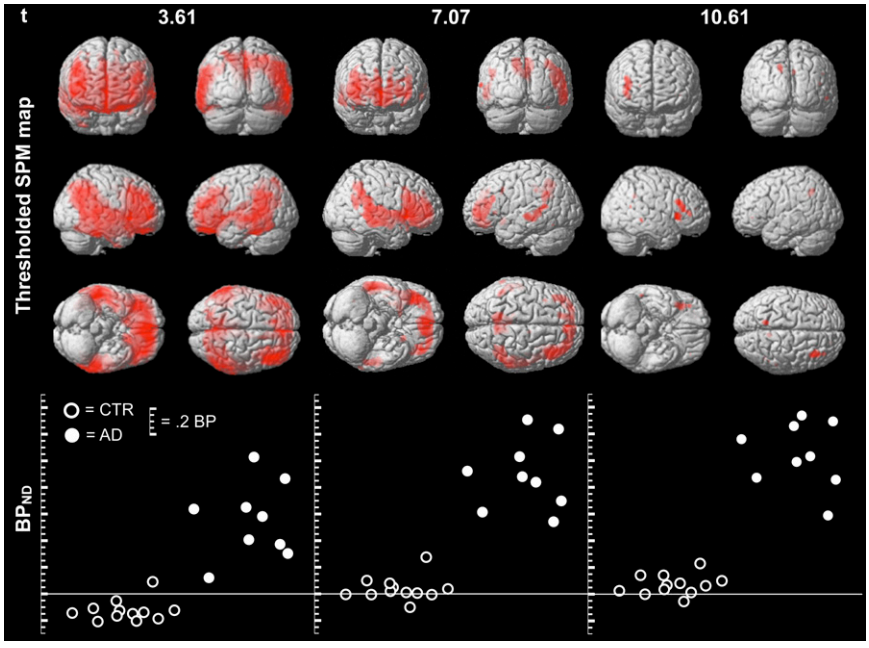

FIGURE 1. Maximum-intensity projections of SPM results comparing control ($n = 12$) and AD ($n = 9$) subjects for several *t* score values. SPM map at each *t* score threshold was used to calculate mean subject cortical BP_{ND}. Scatter plots of mean cortical BP_{ND} in control and AD groups are shown on bottom. Greater separation between groups with increasing *t* threshold is demonstrated. CTR = control.

thresholds are shown in Figure 2A. Group separation increases (decreasing *P* value) as a function of *t* score threshold (Fig. 2A). This increase is evident in the 3 representative scatter plots in Figure 1. The greatest *P* value for comparison of the 2 groups occurs at a *t* score of 10.61. This trough corresponds to a VOI that is 3,376 mm^3 (422 voxels) in MNI space (Fig. 2B). At this size, the VOI consists of several clusters (excluding clusters with <10 voxels) of the following location and volume: right frontal lobe (1,632 mm^3), left precuneus (608 mm^3), right precuneus (184 mm^3), right insular cortex (848 mm^3), and right temporal lobe (80 mm^3). As VOI volume decreases beyond this point, the separation begins to degrade and eventually (Fig. 2B, second to last point, 104 mm^3, 13 voxels) is worse than using most of the brain as a VOI (Fig. 2B, first point, 2.8E6 mm^3, 3.6E5 voxels).

Validation of Data-Derived VOIs in a Second Cohort

After determination of the best *t* score–based VOI map for separating the groups ($t = 10.61$), the VOI was applied to all the subjects to calculate mean cortical BP_{ND} values. Scatter plots of the data obtained from each subject's MR-BP_{ND}-PVC images for the first and second cohorts are shown in Figure 3. The workflow for deriving these data is shown in Figure 4. Comparing control and AD groups from the second cohort resulted in complete separation of the 2 groups ($P < 0.02$), representing 100% sensitivity and specificity.

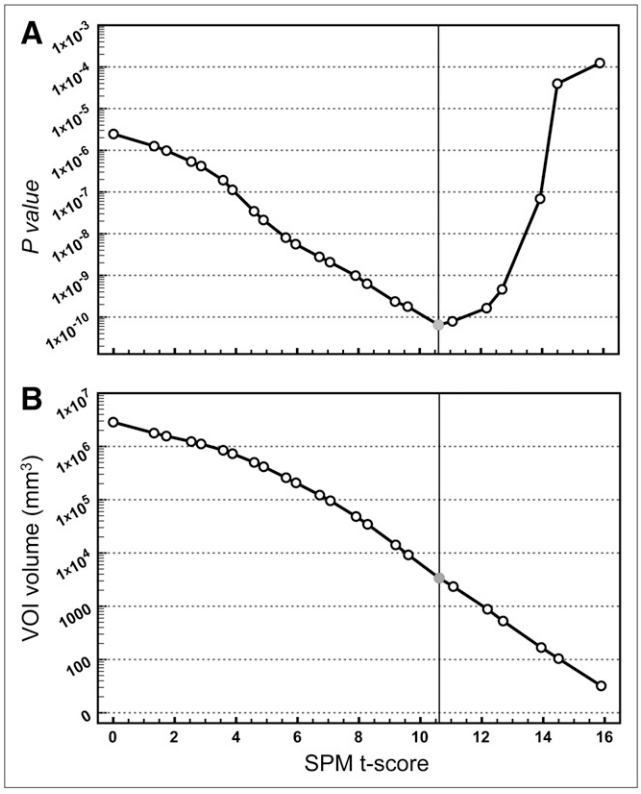

FIGURE 2. Effect of SPM map *t* score threshold on control vs. AD separation (*P* value) and VOI volume. SPM map was derived from control ($n = 12$) and AD ($n = 9$) partial-volume–corrected BP_{ND} voxel images. Map was thresholded at various *t* scores and reapplied as VOIs to MRI space BP_{ND} voxel maps to calculate mean cortical BP_{ND}. *P* values were calculated by performing Student *t* test on control and AD groups mean cortical BP_{ND} for each *t* score threshold (A). Optimal *t* score for separation of groups is 10.61. (B) VOI volume vs. *t* score. Increasing *t* score decreases VOI volume. VOI volume (3,376 mm^3, 422 voxels) at *P* value inflection point is shown (B). *t* score of 10.61 is represented by circle and horizontal black line.

DISCUSSION

We have demonstrated that ^{11}C-PIB BP_{ND} images can be used to create a standardized data-derived or empiric set of VOIs to be used to confirm clinical diagnosis without the need to define conventional anatomic structures on an individual patient's PET scan. The standardized template was created by performing group analysis on a first cohort of control and AD subjects in SPM. The resulting *t* map revealed a significant (uncorrected, $P < 1E-4$) difference in a contiguous cortical area that spanned conventional anatomic regions. The *t* map that contained most of the brain when thresholding at a *t* score of 1.37 ($P < 0.01$, uncorrected) showed almost complete separation between controls and AD, with a slight overlap. By empirically testing *t* score thresholds, we determined that the best *t* score of 10.61 ($P < 1E-9$, uncorrected) results in complete and the greatest separation between controls and AD. Applying this best *t* score thresholded *t* map as a binary VOI to a second cohort of subjects resulted in complete group separation ($P < 0.02$), displaying 100% specificity and sensitivity.

Thresholded *t* Map as a VOI

We derived what essentially is a cortical VOI that is optimized between sampling location and volume. All groups thus far have reported SPM results from control and AD group analysis that determine significant areas of difference (*7,12,24*). SPM maps alone do not aid in diagnosing or classifying an individual subject but rather describe the group effect. On the ROI level, the prefrontal cortex, caudate, and precuneus gyrus have shown the greatest discrimination between controls and patients with AD. For any 1 anatomic ROI, overlap between groups has been reported (*4–7,12*). Others have attempted to avoid this overlap by using mean cortical binding in several regions (*5,6,12*). Although some groups have found that this method ideally separates control and AD groups (*5*), others found that group overlap persists (*6,12*). The success of the cortical binding metric is ultimately dependent on the regions selected. The possibility of establishing an ideal diagnostic anatomic VOI set has not, to our knowledge, been evaluated. Our cortical VOI has been derived empirically to maximize the separation between groups. Unlike previously reported mean-cortical metrics, this VOI avoids rater variability, availability, and time. It can be used with a single subject's MRI and PET scans, and the result is available within hours. An example of how this technique would be applied to an individual subject is presented in Figure 4.

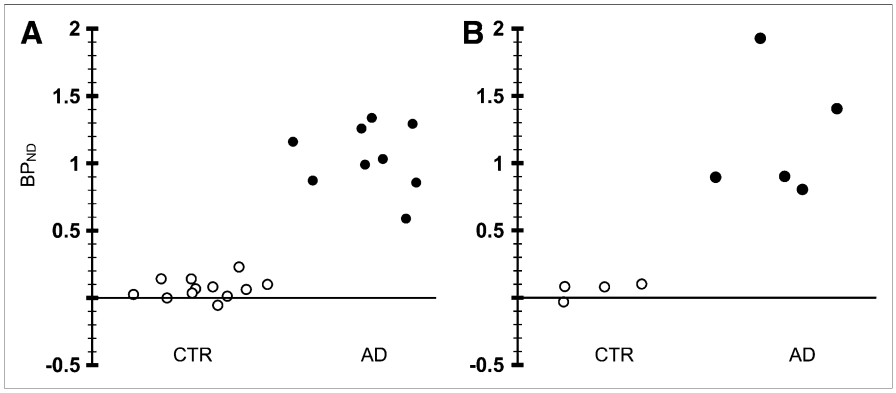

FIGURE 3. Mean cortical BP_{ND} within VOI derived from SPM *t* map thresholded at *t* score of 10.61 (from Fig. 2). VOI was reapplied to first cohort of controls (n = 12) and patients with AD (n = 9) (A) and applied to second cohort of controls (n = 4) and patients with AD (n = 5) (B). CTR = control.

VOI Spatial Distribution

Our map is subject to 3 main sources of variability: location of clusters, volume of each cluster, and laterality.

Peak value coordinates within clusters in our VOI (Fig. 3, t = 10.61) corresponded to frontal, parietal, insular, temporal, and precuneus cortices. Aside from the insular cortex, these regions have been observed to have a high ^{11}C-PIB retention in SPM and ROI analysis. The insular cortex has been implicated in both pathology (*34*) and atrophy (*35*) of patients with AD. Because of the atrophy of this region, partial-volume correcting of our data might have recovered significant signal in this area.

Optimization on the basis of *t* scores relies on keeping voxels that exhibit larger control or AD separation. This optimization is represented by the decreasing *P* value relative to the increasing *t* score (Fig. 3A). An inherent consequence of increasing the *t* score is decreasing VOI sampling volume (Fig. 3B). Smaller VOIs are more specific but also more susceptible to noise. Our VOI consists of 11 disjoint clusters (Fig. 1, t = 10.61), sampling small areas within larger anatomic structures. Though they are relatively small individually, their combined VOI (3,372 mm^3) is comparable to the average left or right hippocampus volume (~3,058 mm^3) of our subjects (data not shown). Template-based hippocampus ROIs have been successfully applied to AD PET data (*36*), suggesting that this volume is sufficient for its use here. Furthermore, our VOI is larger than the hippocampus and is gray matter–corrected on an

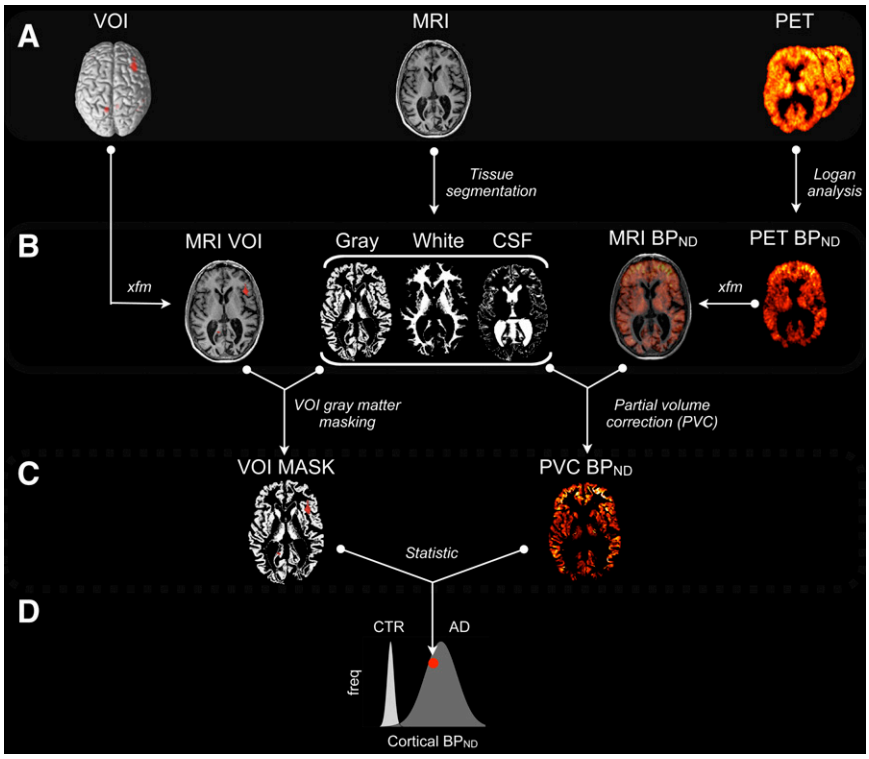

FIGURE 4. Workflow for calculating VOI binding, and potentially diagnosing subject, using our data-derived VOI and novel subjects' MRI and ^{11}C-PIB PET scans (A). (B) VOI is inverse-transformed (xfm) into MRI space using parameters from MRI to MNI normalization. MRI is then segmented into gray, white, and CSF images. PET data is modeled with Logan method to derive BP_{ND} voxel map. BP_{ND} map is inverse-transformed into MRI space using parameters from PET to MRI coregistration. (C) MRI VOI is masked to remove non–gray matter voxels. PVC is applied to BP_{ND} map. (D) Average BP_{ND} value within gray matter VOI voxels is calculated to extract final cortical BP_{ND} measure. Result (red dot) can be compared with control and AD group results derived with same process. CTR = control.

individual basis before calculation of mean cortical binding. Gray matter correction has been shown to reduce white matter and CSF noise in small atlas-based regions (*37*).

The VOI exhibits significant right lateralization (Fig. 1, $t = 10.61$), which has been previously reported in ^{11}C-PIB SPM voxel analysis using data from 10 AD and 11 control subjects (*24*). Our SPM cohort consisted of a comparable 9 AD and 12 control subjects. We concur with the findings of this study (*24*) that right lateralization is not necessarily concomitant with pathology but most likely a result of a small subject dataset. We explored our observation by performing a 3-fold cross-validation by generating new SPM maps from randomly selected groups of 8 controls and 8 patients with AD (data not shown). All maps were examined at their optimal t score threshold. The 3 maps had total VOI volumes of 496 mm^3, 1,328 mm^3, and 2,808 mm^3. We observed right lateralization in 2 of the validation samples but not the third, suggesting this is related to the relatively small sample size. When tested on SPM-naïve data, all of the maps resulted in nonoverlapping control and AD mean cortical binding. On the basis of the variability of these results, the clusters in our VOIs should be considered exploratory. A larger sample is required to create a fully optimized VOI. We are currently gathering data for a more extensive cross-validation analysis to qualify voxels included, as well as to test how the VOI is affected with the addition of more subjects.

VOI PVC

To qualify the use of PVC, we applied our SPM VOI to the second cohort of subjects' corrected and noncorrected BP_{ND} voxel images. The separation between control and AD groups on the basis of the Student t test was 0.0045 for the corrected, compared with 0.0065 for the noncorrected case (data not shown). The larger separation (smaller P value) for the partial-volume–corrected data suggests that correction should be applied, or at least not easily disregarded. Several studies have reported AD or near AD levels of ^{11}C-PIB retention in PIB-positive or older controls (*4–6,23*) and patients with mild cognitive impairment (*5,11,23,38*). PVC should be explored in large sample sizes that include such patients to see if their classification is improved. Our results suggest that partial-volume correcting of voxel images before using them for diagnostic purposes aids in classification. We are collecting additional data from controls, patients with AD, and patients with mild cognitive impairment to further analyze the effectiveness of PVC.

SPM Analysis

Previously reported group voxel analysis has demonstrated that whether using standardized uptake values (*7*) or BP_{ND} (*7,12,24*) as an outcome measure, significance reported in Talairach coordinate space is consistent with conventional anatomic ROI findings. Statistical thresholds (P values) and corrections for multiple comparisons (false discovery rate, familywise error) have also been evaluated (*24*), and it was found that significance in areas of interest is retained. Thus, groups have been reporting significance based on uncorrected (*12*) or corrected (*7*) P values. Because we primarily used P values and t scores to threshold the SPM map, correction was not required.

Processing, Automation, and Future Evaluation

It is essential that a classification method not be cumbersome or difficult to operate, especially in a clinical environment. Although our proposed method is currently not optimal, this preliminary work was designed to qualify the use of PIB voxel data in control and AD discrimination. Many aspects of our design can and should be improved before being used as a reliable clinical or research tool.

Several notable analysis complexities include PET scan duration, processing time, MRI availability, and cerebellar delineation. The reproducibility of using 90-min PET data for quantification has been previously demonstrated (*11*) and is essential for further VOI validation in longitudinal studies. Simplified methods such as 40- to 60-min standardized uptake values or a 60-min Logan method would require further validation against more complex and reliable methods.

Processing time is another important consideration. Currently, once the MRI and PET images have been acquired, total processing time for our method takes 2.5 h (1.5 h for manual cerebellar delineation and 1-h processing on a 3-GHz Xeon machine [Intel]). This requirement can be potentially decreased in 2 ways: by using automated cerebellar labeling and by upgrading hardware. Automated cerebellar-labeling protocols have been available for some time (i.e., FreeSurfer [Athinoula A. Martinos Center for Biomedical Imaging], LONI Atlases [Laboratory of Neuro Imaging, UCLA], SUIT [Jörn Diedrichsen, Human Motor Control Lab, University of Wales Bangor], etc.). Once a suitable method is determined, it can be initiated as soon as the subjects' MR image is acquired so that it is ready before PET acquisition and reconstruction is complete. Personal computer systems with up to 8 processors are now available, some with individual processors as fast as 3.8 GHz. Our software is capable of taking advantage of multiple faster processors that would increase speed now and with future technologic hardware advances. We are currently evaluating existing automatic cerebellar-labeling methods with a cerebellar atlas created from our 16 control brains, and are improving the processing speed of our software. Furthermore, the cerebellar ROI and our software will be freely available online (http://brainimagers.info/home/projects/alzheimers) to facilitate independent analysis and validation. This software can also be used in conjunction with data from the Alzheimer's Disease Neuroimaging Initiative database (http://www.loni.ucla.edu/ADNI).

CONCLUSION

The derivation and use of a standardized VOI has been found to be a robust metric for AD diagnosis made on the basis of ^{11}C-PIB data. The VOI, compared with any metric that has previously been published, demonstrates the same or better discrimination capabilities and can be made totally

automatic, avoiding human error. Before using this VOI in a clinical setting, however, several issues should be addressed. First, the small number of test subjects is not enough to cover all cases, especially the borderline controls or patients with AD. Second, the signal and separation could potentially be increased by using an arterial input function. Third, the signal could be increased further by using a modeling scheme that does not have a noise-dependent bias. Finally, the cerebellum is the only region that requires manual identification. This region could potentially be replaced with a template version, making this analysis fully automated. Although further evaluation is necessary, these results provide an automated basis for making the distinction between patients with AD and healthy control subjects using ^{11}C-PIB. Such a robust metric may improve diagnosis or may be used to select patients with confirmed amyloid deposition for clinical trials involving novel drugs aimed at reducing amyloid load in AD. Evaluation of this method in patients with mild cognitive impairment would be important to assess its ability in predicting conversion to AD.

ACKNOWLEDGMENTS

We thank Yani Pan for meticulously labeling MR images and Dr. Arno Klein, David Andrews, and Kevin DeSimone for their exhaustive insight in illustration design. This study was supported by a grant from the National Institutes of Health (R01AG017761) and research support from GlaxoSmithKline (GSK). Drs. Libri, Upton, Lai, and Gunn are GSK employees and report owning shares in GSK but declare that they have no financial interest in or financial conflict with the subject matter or materials discussed in this article.

REFERENCES

1. Minino AM, Heron MP, Murphy SL, Kochanek KD, Centers for Disease Control and Prevention National Center for Health Statistics National Vital Statistics System. Deaths: final data for 2004. *Natl Vital Stat Rep.* 2007;55:1–119.
2. Zamrini E, De Santi S, Tolar M. Imaging is superior to cognitive testing for early diagnosis of Alzheimer's disease. *Neurobiol Aging.* 2004;25:685–691.
3. Thal DR, Rub U, Orantes M, Braak H. Phases of Aβ-deposition in the human brain and its relevance for the development of AD. *Neurology.* 2002;58:1791–1800.
4. Klunk WE, Engler H, Nordberg A, et al. Imaging brain amyloid in Alzheimer's disease with Pittsburgh Compound-B. *Ann Neurol.* 2004;55:306–319.
5. Rowe CC, Ng S, Ackermann U, et al. Imaging beta-amyloid burden in aging and dementia. *Neurology.* 2007;68:1718–1725.
6. Mintun MA, Larossa GN, Sheline YI, et al. [^{11}C]PIB in a nondemented population: potential antecedent marker of Alzheimer disease. *Neurology.* 2006;67:446–452.
7. Kemppainen NM, Aalto S, Wilson IA, et al. Voxel-based analysis of PET amyloid ligand [^{11}C]PIB uptake in Alzheimer disease. *Neurology.* 2006;67:1575–1580.
8. Zhou Y, Resnick SM, Ye W, et al. Using a reference tissue model with spatial constraint to quantify [^{11}C]Pittsburgh compound B PET for early diagnosis of Alzheimer's disease. *Neuroimage.* 2007;36:298–312.
9. Kanetaka H, Matsuda H, Asada T, et al. Effects of partial volume correction on discrimination between very early Alzheimer's dementia and controls using brain perfusion SPECT. *Eur J Nucl Med Mol Imaging.* 2004;31:975–980.
10. Rousset OG, Ma Y, Evans AC. Correction for partial volume effects in PET: principle and validation. *J Nucl Med.* 1998;39:904–911.
11. Lopresti BJ, Klunk WE, Mathis CA, et al. Simplified quantification of Pittsburgh Compound B amyloid imaging PET studies: a comparative analysis. *J Nucl Med.* 2005;46:1959–1972.
12. Ng S, Villemagne VL, Berlangieri S, et al. Visual assessment versus quantitative assessment of ^{11}C-PIB PET and ^{18}F-FDG PET for detection of Alzheimer's disease. *J Nucl Med.* 2007;48:547–552.
13. McKhann G, Drachman D, Folstein M, Katzman R, Price D, Stadlan EM. Clinical diagnosis of Alzheimer's disease: report of the NINCDS-ADRDA Work Group under the auspices of Department of Health and Human Services Task Force on Alzheimer's Disease. *Neurology.* 1984;34:939–944.
14. Parsey RV, Sokol LO, Belanger MJ, et al. Amyloid plaque imaging agent [C-11]-6-OH-BTA-1: biodistribution and radiation dosimetry in baboon. *Nucl Med Commun.* 2005;26:875–880.
15. Watson CC, Newport D, Casey ME. A single scatter simulation technique for scatter correction in 3D PET. In: Grangeat P, Amans J-L, eds. *Three Dimensional Image Reconstruction in Radiology and Nuclear Medicine.* Dordrecht, The Netherlands: Kluwer Academic; 1996:255–268.
16. Mawlawi O, Martinez D, Slifstein M, et al. Imaging human mesolimbic dopamine transmission with positron emission tomography: I. Accuracy and precision of D_2 receptor parameter measurements in ventral striatum. *J Cereb Blood Flow Metab.* 2001;21:1034–1057.
17. Jenkinson M, Smith S. A global optimisation method for robust affine registration of brain images. *Med Image Anal.* 2001;5:143–156.
18. Smith SM. Fast robust automated brain extraction. *Hum Brain Mapp.* 2002;17:143–155.
19. Ashburner J, Friston KJ. Nonlinear spatial normalization using basis functions. *Hum Brain Mapp.* 1999;7:254–266.
20. Ashburner J, Friston KJ. Unified segmentation. *Neuroimage.* 2005;26:839–851.
21. Logan J, Fowler JS, Volkow ND, Wang GJ, Ding YS, Alexoff DL. Distribution volume ratios without blood sampling from graphical analysis of PET data. *J Cereb Blood Flow Metab.* 1996;16:834–840.
22. Joachim CL, Morris JH, Selkoe DJ. Diffuse senile plaques occur commonly in the cerebellum in Alzheimer's disease. *Am J Pathol.* 1989;135:309–319.
23. Price JC, Klunk WE, Lopresti BJ, et al. Kinetic modeling of amyloid binding in humans using PET imaging and Pittsburgh Compound-B. *J Cereb Blood Flow Metab.* 2005;25:1528–1547.
24. Ziolko SK, Weissfeld LA, Klunk WE, et al. Evaluation of voxel-based methods for the statistical analysis of PIB PET amyloid imaging studies in Alzheimer's disease. *Neuroimage.* 2006;33:94–102.
25. Logan J, Fowler JS, Volkow ND, Ding YS, Wang GJ, Alexoff DL. A strategy for removing the bias in the graphical analysis method. *J Cereb Blood Flow Metab.* 2001;21:307–320.
26. Kimura Y, Naganawa M, Shidahara M, Ikoma Y, Watabe H. PET kinetic analysis: pitfalls and a solution for the Logan plot. *Ann Nucl Med.* 2007;21:1–8.
27. Hoffman EJ, Huang SC, Phelps ME. Quantitation in positron emission computed tomography: 1. Effect of object size. *J Comput Assist Tomogr.* 1979;3:299–308.
28. Chetelat G, Landeau B, Eustache F, et al. Using voxel-based morphometry to map the structural changes associated with rapid conversion in MCI: a longitudinal MRI study. *Neuroimage.* 2005;27:934–946.
29. Meltzer CC, Zubieta JK, Brandt J, Tune LE, Mayberg HS, Frost JJ. Regional hypometabolism in Alzheimer's disease as measured by positron emission tomography after correction for effects of partial volume averaging. *Neurology.* 1996;47:454–461.
30. Muller-Gartner HW, Links JM, Prince JL, et al. Measurement of radiotracer concentration in brain gray matter using positron emission tomography: MRI-based correction for partial volume effects. *J Cereb Blood Flow Metab.* 1992;12:571–583.
31. Meltzer CC, Kinahan PE, Greer PJ, et al. Comparative evaluation of MR-based partial-volume correction schemes for PET. *J Nucl Med.* 1999;40:2053–2065.
32. Mazziotta JC, Toga AW, Evans A, Fox P, Lancaster J. A probabilistic atlas of the human brain: theory and rationale for its development. The International Consortium for Brain Mapping (ICBM). *Neuroimage.* 1995;2:89–101.
33. Mazziotta J, Toga A, Evans A, et al. A probabilistic atlas and reference system for the human brain. International Consortium for Brain Mapping (ICBM). *Philos Trans R Soc Lond B Biol Sci.* 2001;356:1293–1322.
34. Royall DR, Gao JH, Kellogg DL Jr. Insular Alzheimer's disease pathology as a cause of "age-related" autonomic dysfunction and mortality in the non-demented elderly. *Med Hypotheses.* 2006;67:747–758.
35. Foundas AL, Eure KF, Seltzer B. Conventional MRI volumetric measures of parietal and insular cortex in Alzheimer's disease. *Prog Neuropsychopharmacol Biol Psychiatry.* 1996;20:1131–1144.
36. Mosconi L, Tsui WH, De Santi S, et al. Reduced hippocampal metabolism in MCI and AD: automated FDG-PET image analysis. *Neurology.* 2005;64:1860–1867.
37. Rusjan P, Mamo D, Ginovart N, et al. An automated method for the extraction of regional data from PET images. *Psychiatry Res.* 2006;147:79–89.
38. Kemppainen NM, Aalto S, Wilson IA, et al. PET amyloid ligand [^{11}C]PIB uptake is increased in mild cognitive impairment. *Neurology.* 2007;68:1603–1606.